JCTC Journal of Chemical Theory and Computation

Molecular Dynamics Simulations of Solvation and Solvent Reorganization Dynamics in CO_2-Expanded Methanol and Acetone

John L. Gohres,[†,§,||] Alexander V. Popov,[‡,||] Rigoberto Hernandez,*[,‡,§,||] Charles L. Liotta,[†,‡,§] and Charles A. Eckert*[,†,‡,§]

School of Chemical & Biomolecular Engineering, School of Chemistry & Biochemistry, Specialty Separations Center, and Center for Computational and Molecular Science and Technology, Georgia Institute of Technology, Atlanta, Georgia 30332-0100

Received August 28, 2008

Abstract: Composition-dependent solvation dynamics around the probe coumarin 153 (C153) have been explored in CO_2-expanded methanol and acetone with molecular dynamics (MD) simulations. Solvent response functions are biexponential with two distinct decay time scales: a rapid initial decay (~0.1 ps) and a long relaxation process. Solvation times in both expanded solvent classes are nearly constant at partition compositions up to 80% CO_2. The extent of solvation beyond this composition has the greatest tunability and sensitivity to bulk solvent composition. Solvent rotational correlation functions (RCFs) have also been used to explore rotational relaxation. Rotations have a larger range of time scales and are dependent on a number of factors including bulk composition, solvent-solvent interactions, particularly hydrogen bonding, and proximity to C153. The establishment of the solvation structure around a solute in a GXL is clearly a complex process. With respect to the local solvent domain around C153, it was seen to be primarily affected by a nonlinear combination of the rotational and diffusive transport dynamics.

1. Introduction

Gas-expanded liquids (GXLs) are a leading candidate for next-generation tunable solvents and are formed by the dissolution of appreciable amounts of gas into an organic liquid. The resulting mixture is a volume-expanded liquid phase with tunable physical and solvation properties like dielectric constant and viscosity.[1,2] An inherent advantage of GXLs results from the increase in gas (H_2, O_2) solubility in the liquid phase. Relative to neat organic solvents, GXLs have improved yield and selectivity of homogeneously catalyzed oxidation reactions.[3] A significant amount of research has shown that GXLs are advantageous over organic solvents for a variety of reactions,[4−9] extractions,[10] and materials processing applications.[11−18] Consequently a great deal of effort has focused on understanding the molecular-scale properties of GXLs so to fully exploit their unique solvent properties.

Electronic excitation of the laser dye Coumarin 153 (C153) creates an excited-state dipole moment nearly 9 Debye greater than the ground-state dipole moment.[19] Recent spectroscopic and molecular dynamics (MD) simulation results showed organic enrichment around C153 in CO_2-expanded solvents.[20−22] Different solvation patterns between the ground and excited states of C153, specifically organic and CO_2 density enhancements relative to the ground-state cause a solvent relaxation process to solvate the excited C153. Solvent relaxation consists of electronic and nuclear rearrangements with time scales that are dependent on bulk solvent properties and molecular interactions. MD simulations provide a direct comparison to time-resolved fluorescence and give molecular-level insight into solvation mechanisms that compose solvent reorganization. Many studies

* Corresponding author e-mail: cae@gatech.edu.
† School of Chemical & Biomolecular Engineering.
§ Specialty Separations Center.
|| Center for Computational and Molecular Science and Technology.
‡ School of Chemistry & Biochemistry.

10.1021/ct800353s CCC: $40.75
Published on Web 01/14/2009

have explored solvation dynamics in tunable solvents with experimental and computational techniques[23−27] because solvent dynamics affect chemical reactions.[28]

Solvent dynamics impact ultrafast processes like electron-transfer and free-radical reactions. Recent studies have shown that solvent polarity affects the degree of polymerization of copper-catalyzed radical polymerizations.[29,30] The formation of halide ions (from halide radicals) and the subsequent coordination to the copper center is directly related to the solvent medium. Solvents that can solvate the newly created halide ion have a lower coordination equilibrium constant and ultimately better molecular weight control. Electron tunneling through a donor-bridge-acceptor dyad is a direct function of solvent environment. The solvent reorganization energy impacts the ease of electron transfer and affects the optical properties and performance of the dyad.[31−33] GXLs are attractive solvents for dyads and other electronic materials because the solvent environment can be manipulated by CO_2 adjustments, allowing *in situ* control of charge transfer or a free radical polymerization.

In this manuscript, the reorganization dynamics and rotational dynamics of a solvent around a probe within two GXLs—methanol and acetone—are explored using MD simulations through a range of bulk compositions. The primary challenge in simulating these systems emerges from the difficulty of describing true dynamics in multiphase systems within cell sizes that are amenable to current computer infrastructure. Rigorous multiphase ensemble approaches[34] have been performed by other groups in order to obtain the phase diagram as well as to vet the quality of the underlying potentials.

While resolving these critical questions, such Monte Carlo based approaches do not provide dynamic information. An alternative approach taken by us[35] and Maroncelli and coworkers[36] has focused on the single solution phase on which a microscopic volume may be modeled using molecular dynamics. The appropriate constraints on this unit cell—such as volume, temperature, and relative composition of cosolvents—must be obtained either by the multiphase simulations or semiempirically using experimental data. In previous work, we have found that the quality of the underlying potentials employed in the simulations appears to be sufficient to be in agreement with the experimentally obtained phase diagram and hence have focused only on the use of MD simulations to reveal the structure and dynamics in a GXL phase. The present work goes further by calculating structural and rotational correlations resulting from electronic excitation of the solute. The results demonstrate the versatile nature of GXLs in providing solvent design tools for materials processing applications and free radical and electron transfer reactions.

2. Computational Methods

Solvation involves both electronic and nuclear rearrangements. Solute repolarization (beyond the changes in the charge distribution from the ground to excited state) was not examined in this work as it should be a higher order correction to the primary changes in the response function due to the significant charge redistribution from the ground to excited states. Polarization effects generally slow down the solvent response in polar solvents.[37] As CO_2 is added, the solvent structure becomes increasingly nonpolar, and thereby further reduces the role of repolarization. On the other hand, nuclear motions like solvent rotation and translation have a large impact on the response function. A typical solvent response in GXLs has two distinct time scales: a fast inertial decay period that typically accounts for ∼75% of the loss in correlation and a slow long-term relaxation. The inertial decay is very fast and presumably dominated by rotation. The translational diffusion does not contribute significantly because the local density autocorrelation function observed by Shukla et al.[35] is much slower (∼10−80 ps) than the solvation time found here (∼1−10 ps). The relative speed of this solvation is due to preferential solvation of the initial and final states as will be seen in the results below. C153 rotation and translation is slow relative to the solvent atoms because of its large size and does not contribute to the relaxation process.

An investigation of the mechanical response to different solvation events provides insight into the molecular interactions and solvent properties that determine the solvent response. These are surmised by the solvent response function described in Section 2.2. However, these necessarily contain a component due simply to rotational response in the neat solvent. Hence rotational correlation functions—described in Section 2.3—must also be obtained so as to resolve the dynamics effects due to a given solute.

2.1. Model Parameterization and Methods. All simulations have been run using the DL_POLY v2.0[38] computer suite. It implements the Verlet leapfrog algorithm to integrate the equations of motion. All molecules are treated as rigid bodies interacting with each other through a Lennard-Jones plus Coulombic interactions force field. Specifically, C153 has been modeled with an OPLS-AA force field[39] whose partial charges are taken from Kumar and Maroncelli.[40] MeOH and acetone pair interactions have been treated by the 3-site J2[41] and 4-site OPLS[42] force fields, respectively, and CO_2 pair interactions employed the 3-site TraPPE potential.[34] The methyl groups in MeOH and acetone are treated as united-atom groups in these force fields. Site−site interactions between sites on a mixed pair of molecules are determined by the Lorentz−Berthelot combining rules: $\sigma_{12} = 0.5(\sigma_1 + \sigma_2)$ and $\varepsilon_{12} = (\varepsilon_1\varepsilon_2)^{0.5}$.

Simulations are performed on a unit cell with periodic boundary conditions at a density coincident with the liquid phase of the corresponding GXL following the procedure described in prior work.[35] As described in the Introduction, this construct is metastable in the sense that it is single-phase and presumably at higher energy than the condition which would split into two phases. However, the system is constrained such that the splitting is inaccessible during the simulations. The initial configuration for equilibration runs is a randomly distributed periodic box of 500 solvent molecules (600 for 98% CO_2 GXLs) and a single C153 in the ground state. The box size has been scaled to match the liquid-phase volumes as predicted by the Patel-Teja equation of state.[43] Starting from equilibrated structures, the ensemble of initial configurations (needed for the nonequilibrium

simulations) is obtained by sampling structures every 6 ps during long NVT trajectories of the ground-state (S_0) electronic configuration of C153 and solvent. Representative correlation functions and structures were initially obtained from simulations performed at various timesteps and seen to converge at 3 fs; hence all the reported simulations were performed with 3 fs timesteps. The temperature has been maintained at 300 K with a Nose-Hoover thermostat whose relaxation time is 1 ps. Nonequilibrium trajectories are initialized at each of the configurations from the equilibrium ensemble, but C153 is instantaneously placed on the S_1 excited-state—assuming Franck−Condon transitions—by replacing the partial charges in the molecular mechanics force field from the ground-state to excited-state values. They are usually propagated for 9 ps under NVE conditions as this was found to be sufficient to capture most of the nonzero correlation function; but they were propagated up to 20 ps when necessary. Coordinates are saved every 45 fs and analyzed using an external FORTRAN program.

2.2. Solvent Response Function (SRF). Solvation dynamics are explored through the solvent response function (SRF)

$$S(t) = \frac{\Delta E(t) - \Delta E(\infty)}{\Delta E(0) - \Delta E(\infty)} \tag{1}$$

where $\Delta E(t)$ is the energy gap between the C153 electronic states and $S(t)$ is the SRF. The SRF is a normalized function of the energy gap between the C153 electronic states and is a measure of total solvent−solute interaction energy between the electronic states. For simplicity, the C153 Lennard-Jones parameters were assumed constant in the ground and excited states. Therefore, the energy gap is composed of the electrostatic interaction between the solvent and solute and can be written as

$$\Delta E = \frac{1}{4\pi\varepsilon_0}\sum_{i}^{N}\sum_{\alpha}\sum_{\beta}\frac{\Delta q_\alpha q_{i\beta}}{r_{\alpha,i\beta}} \tag{2}$$

where ε_0 is the relative permittivity in vacuum, N is the number if solvent molecules, α denotes a solute atom, and $i\beta$ denotes solvent atom β on molecule i. Terms $q_{i\beta}$ and Δq_α are respectively the partial charge on solvent atom β and difference in partial charge between ground and excited-state on C153 atom α. The nonequilibrium response can be connected to equilibrium fluctuations through the equilibrium time correlation function:

$$C(t) = \frac{\langle \delta E(0)\delta E(t)\rangle}{\langle (\delta E)^2\rangle} \tag{3}$$

A convenient assumption for nonequilibrium simulations is the linear response approximation which provides an estimate for the SRF as $S(t) \cong C(t)$. In this limit, the nonequilibrium response is described by fluctuations around the average, $\delta E(t) = \Delta E(t) - [\Delta E]$, in equilibrium or unperturbed systems. The approximation $S(t) \cong C(t)$ is convenient and reasonable for most neat liquid solvents but breaks down in liquid mixtures with preferential solvation or highly compressible fluids systems like SCFs.[25−27] Preferential solvation and local density enhancements become increasingly pronounced around excited C153, and local density enhancements become larger in magnitude than normal solvent fluctuations. Consequently the linear assumption is not applicable in GXLs because of these local density enhancements. Although the calculation and analysis of nonequilibrium simulations is more cumbersome, it is necessary to obtain the solvation dynamics in GXLs and rotational dynamics of solutes in GXLs following excitation.

2.3. Rotational Correlation Functions (RCFs). Rotational dynamics of the cosolvents —CO_2 and the organic species—have been explored through the first- and second-order rotational correlation functions (RCF)

$$C^{(1)}(t) = \langle \vec{n}(t)\cdot\vec{n}(0)\rangle \tag{4}$$

$$C^{(2)}(t) = \frac{1}{2}\langle 3[\vec{n}(t)\cdot\vec{n}(0)]^2 - 1\rangle \tag{5}$$

where $\vec{n}$ is a characteristic axis vector of an organic or CO_2 molecule, and $C^{(1)}$ and $C^{(2)}$ are the respective first and second ranked RCFs. CO_2 is a linear molecule with one characteristic vector extending from the carbon atom to an oxygen atom. A single axis of rotation is sufficient to describe MeOH rotation—the bond between the oxygen atom and the protic hydrogen. Rotation of a unit vector characterizing this bond contributes more to the solvation response than the oxygen methyl vector since the hydroxyl group is more polar and therefore more responsive to an electric field. Acetone required two axes of rotation because it is a bulky molecule with asymmetric rotations. One vector extends along the carbonyl group from the carbon to the oxygen, and the other is directed from the carbonyl carbon to a methyl group. Two orders of RCFs were used to examine solvent rotation: first-order RCFs—because their decay tends to be dominated by the collective loss of orientation relative to the initial alignment—and second-order RCFs—because their decay tends to be dominated by the loss of molecule's orientation relative to each other.

RCFs of all three solvent molecules are classified within three cases, as delineated by time relative to the excitation and the relative proximity to the C153 probe: 1) rotations of all solvent molecules immediately following C153 excitation—the SRF case; 2) rotations of molecules that are in the local or cybotactic region of C153 after excitation—the Local case; and 3) rotations that occur in the bulk fluid, i.e. no C153 molecule in the simulation—the Bulk case. This classification allows us to distinguish between bulk solvent rotations that result from normal fluctuations and solvent rotations that are affected by C153 excitation. The cybotactic region is a dynamic area that constantly changes location as the solute and solvent molecules diffuse, so assumptions were made to study this transient region. The same definition was used as was described in our previous work.[21] Briefly, a sphere of 7 Å was drawn outward from the C153 center of mass. Any solvent molecules that were initially in this sphere were considered part of the cybotactic region throughout the entire simulation. C153 diffusion is very slow, and most solvent rotations occur before diffusive escape from the region. Solvent molecules that entered the sphere midsimulation were not considered a part of the cybotactic region for simplification purposes.

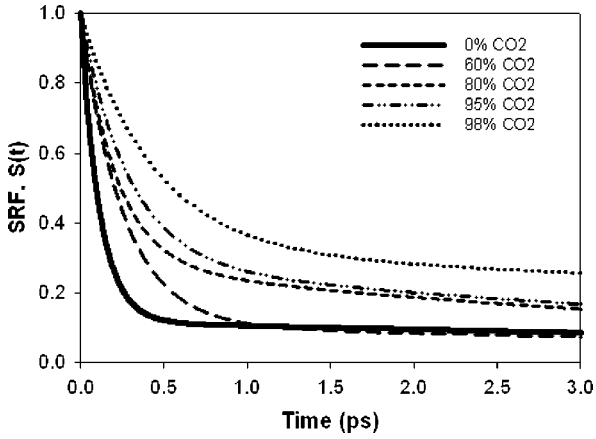

Figure 1. Solvent response functions in neat acetone and CO_2-expanded acetone at varying CO_2 compositions.

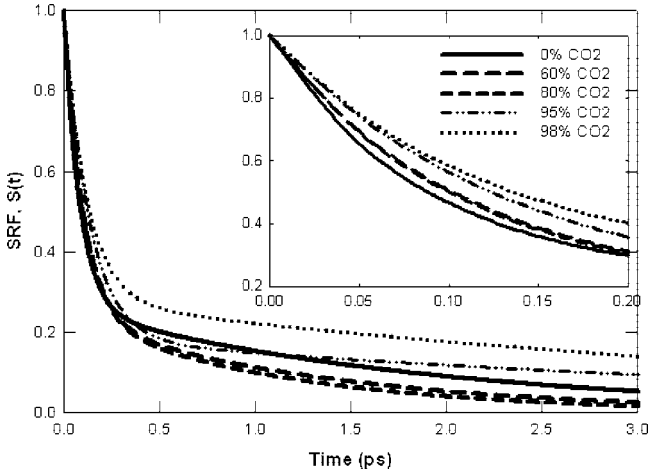

Figure 2. Solvent response functions in neat MeOH and CO_2-expanded MeOH at varying CO_2 compositions. The inset magnifies the initial decay behavior.

3. Results and Discussion

3.1. Solvation Dynamics. Solvent response functions of acetone GXLs and MeOH GXLs, including neat organic liquids, are presented in Figures 1 and 2, respectively. The curves represent the average of over 1000 trajectories fit to a multiexponential decay function

$$S(t) = \sum_{i=1}^{k} a_i \exp(-t/\tau_i) \tag{6}$$

where a_i is a pre-exponential fitting parameter that gives the relative weighting of the time scale and τ_i is a characteristic decay time that is indicative of a different solvation time scale for each of k exponentials. In the present work, k was taken to be no greater than 3, and most of the decay functions were fit well at k equal to 1 or 2. Such fits ignore the earliest ballistic part of the decay function which is nonexponential and essentially hidden at the scale displayed in, for example, Figures 1 and 2. All SRFs were fit within a standard error less than 4% using the parameters given in Table 1. Solvation time quantifies the reorganization process and is found by integrating the fit of the solvation response function as specified by eq 6, yielding

$$\tau_S = \int_0^\infty S(t)\, dt = \sum_{i=1}^{k} a_i \tau_i \tag{7}$$

where τ_s is the effective total solvation time. A plot of solvation time versus CO_2 composition is shown in Figure 3 to illustrate the effects of composition on solvation that are not directly apparent in Figures 1 and 2.

The neat MeOH solvation time, $\tau_S \approx 0.55$ ps, is much faster than the experimental result, $\tau_S \approx 5.0$ ps, found by Horng et al.[19] in the supercritical regime, but it agrees reasonably well with MD simulation results from other researchers.[37,40] Kumar and Maroncelli[40] used a fixed C153 molecule and the linear time-correlation approximation of eq 3 in their analysis. Cichos et al.[37] used a similar approach but added a nonequilibrium case with polarizability. Polarizable force fields slow down the solvent response and provide better agreement with the experimental findings. SRFs in neat acetone ($\tau_S \approx 1.27$ ps) are in better agreement with experimental data[19] ($\tau_S \approx 0.58$ ps) than those in neat MeOH, but this result is slightly slower than the experimental data.

Several interesting features in the SRFs shown in Figures 1−3 suggest that solvation is solvent-dependent, and intermolecular interactions and bulk fluid properties both affect the response time. Solvation times in both GXLs remain stagnant up to ~80% CO_2 before increasing exponentially. The effects of CO_2 are more pronounced in acetone GXLs where the solvent response slows down by nearly 5 ps. Similarly, CO_2 slows down the response at high composition in MeOH GXLs, although the time scale change is approximately 1 ps. This observed difference between the two

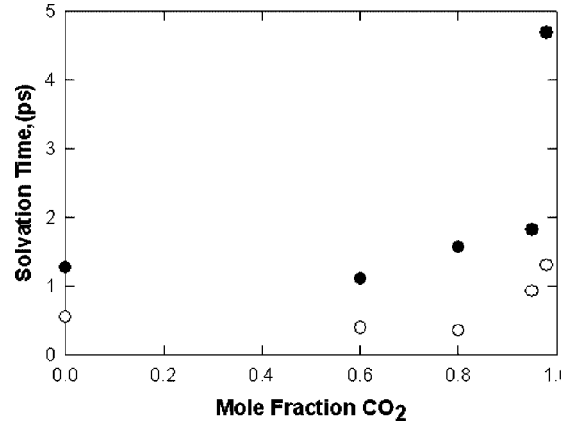

Figure 3. Solvation times in CO_2-expanded acetone (filled circles) and MeOH (open circles).

Table 1. Biexponential Decay Fitting Parameters for SRF in CO_2-Expanded Acetone and MeOH

% CO_2	a_1	τ_1 (ps)	a_2	τ_2 (ps)
neat acetone	0.883	0.112	0.117	10.0
60% in acetone	0.892	0.253	0.108	8.147
80% in acetone	0.722	0.216	0.278	5.074
95% in acetone	0.715	0.288	0.285	5.66
98% in acetone	0.681	0.44	0.319	13.77
neat MeOH	0.739	0.082	0.261	1.874
60% in MeOH	0.763	0.102	0.237	1.338
80% in MeOH	0.759	0.10	0.241	1.126
95% in MeOH	0.815	0.132	0.185	4.443
98% in MeOH	0.72	0.119	0.28	4.358

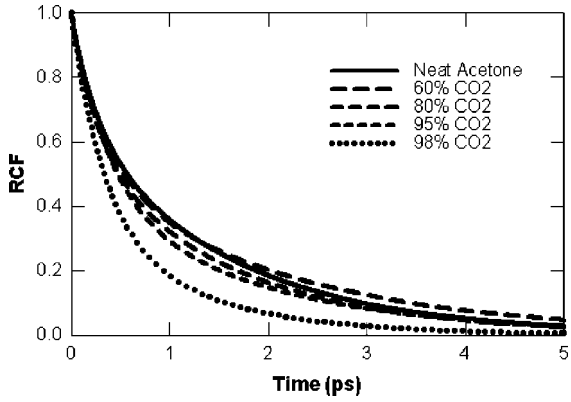

Figure 4. First-order acetone RCFs of the C−O bond in acetone-based GXLs for the SRF case.

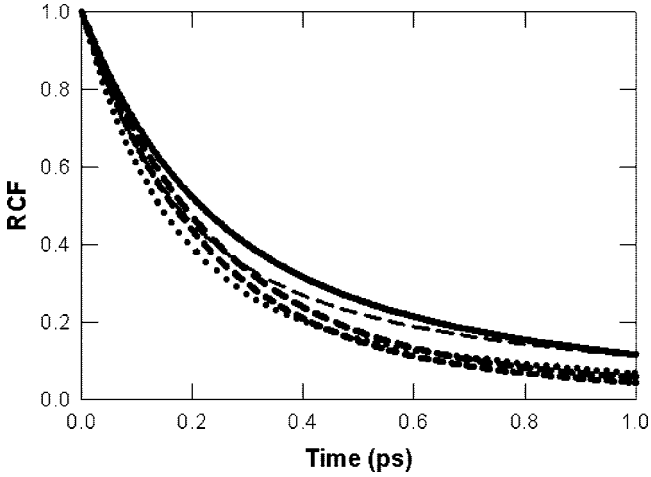

Figure 5. Second-order RCFs for acetone of the C−O bond around the carbonyl bond (SRF case) in neat acetone and various acetone GXLs. Lines represent the same cosolvent mixtures as used in Figure 4.

types of GXLs is directly related to the degree of cosolvent preferential solvation around C153 and its ability to respond to the excited-state dipole moment by realignment. Both acetone and MeOH preferentially solvate both ground and excited-state C153,[21] but there are other differences in molecular structure and solvent properties that could affect the solvent response. MeOH is a smaller molecule than acetone and could in principle diffuse faster than acetone and lead to a packing of more molecules within a local region around C153. MeOH is more polar than acetone and forms hydrogen bonds. Higher polarity causes lower solvation energy which decreases the amount of MeOH required to solvate the excited dipole; however, hydrogen bonding affects MeOH dynamics and could slow down MeOH rotations and diffusion. Thus the solvent response is a complex event that depends on the net effect of multiple factors.

3.2. Solvent Rotation. First- and second-order RCFs (of the C−O bond) for acetone GXLs—SRF case—are shown in Figures 4 and 5. Acetone RCFs of the C-Me bond are provided in Figures S2 and S3 in the Supporting Information. Likewise, first- and second-order RCFs for MeOH GXLs are shown in Figures 6 and 7, respectively. These figures illustrate the increase in rotational relaxation resulting from CO_2 addition. From the perspective of the "GXL" metaphor,

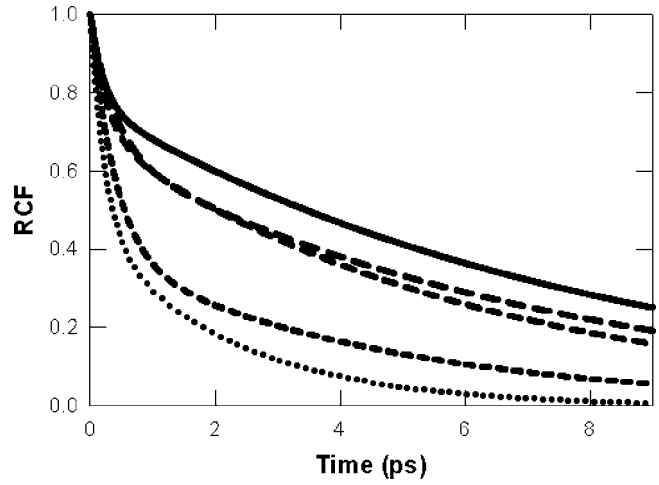

Figure 6. First-order MeOH RCFs (of the MeOH cylindrical symmetry axis) in MeOH-based GXLs for the SRF case. Lines represent the same cosolvent mixtures as used in Figure 4.

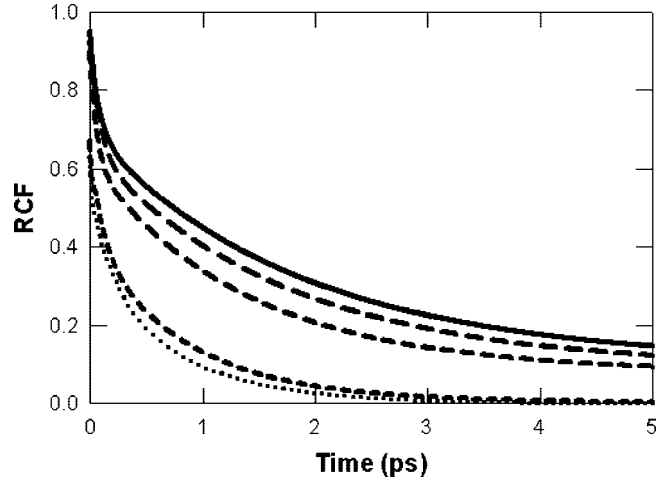

Figure 7. Second-order RCFs for MeOH (of the MeOH cylindrical symmetry axis) in neat MeOH and various acetone GXLs for the SRF case. Lines represent the same cosolvent mixtures as used in Figure 4.

this is not surprising because the increasing presence of CO_2 makes the liquid phase more gaslike and hence increases the (translational and rotational) mobility of solutes. There are several apparent features in these figures that are common throughout all the cases considered: the presence of dynamics at multiple time scales, a rapid initial decay followed by a long-term decay, and a large rate increase between 80% CO_2 and 95% CO_2. In addition, there are two distinguishing features between acetone and MeOH RCFs: 1) initial acetone rotations are nearly identical between all GXLs and neat acetone. This is seen by the overlap of RCFs until 0.3 ps when divergence begins. 2) Acetone rotations are faster than those in MeOH. All acetone RCFs are uncorrelated within 2 ps, while MeOH RCFs indicate correlations in a range from 2 ps to 9 ps. Second-order CO_2 RCFs—SRF case—in acetone and MeOH GXLs are shown in Figures 8 and 9, respectively. First-order CO_2 RCFs can be found in Figures S1 and S4 in the Supporting Information. CO_2 molecules rotate faster than both organic species in the same solvent and are less sensitive

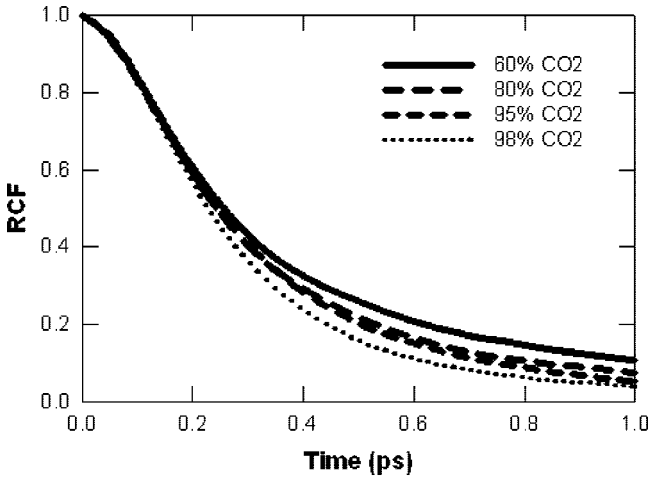

Figure 8. Second-order RCFs for CO_2 molecules in acetone GXLs.

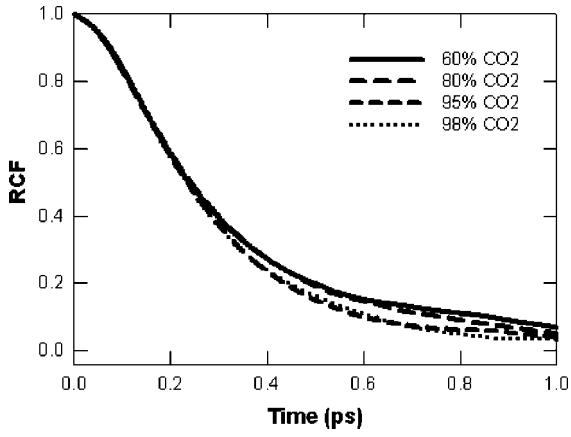

Figure 9. Second-order RCFs for CO_2 molecules in MeOH GXLs.

to bulk composition, although rotations are faster when more CO_2 is present. CO_2 has an initial lag period during the first 0.1 ps that is not present in the organic RCFs. CO_2 could be initially unresponsive because weak intermolecular interactions prevent an initial thrust to start rotation. This time lag, τ_{lag}, can be estimated from an approximation for the velocity autocorrelation function suitable for one-dimensional motion at small times[44]

$$C(t) \approx \exp(-[\sqrt{t^2 + \tau_{lag}^2} - \tau_1]/\tau_1) \quad (8)$$

where τ_1 is the apparent monoexponential decay time. The inflection point for this function, t_{infl}, obeys the equation

$$t_{infl}^2 \sqrt{t_{infl}^2 + \tau_{lag}^2} = \tau_1 \tau_{lag}^2 \quad (9)$$

As can be seen from Figures 8, 9, S3, and S4, t_{infl} is approximately 0.2 ps. With τ_1 ranging from 0.3 to 0.9 ps (Tables S1 and S2), one obtains τ_{lag} in a range from 0.1 ps to 0.2 ps. Note that this lag period corresponds to the average time between collisions, and, as it has already been mentioned, it is larger for CO_2 molecules due to their weak interaction.

All RCFs were fit by a sum of exponential decay functions per eq 6 ignoring the initial very-fast ballistic component.

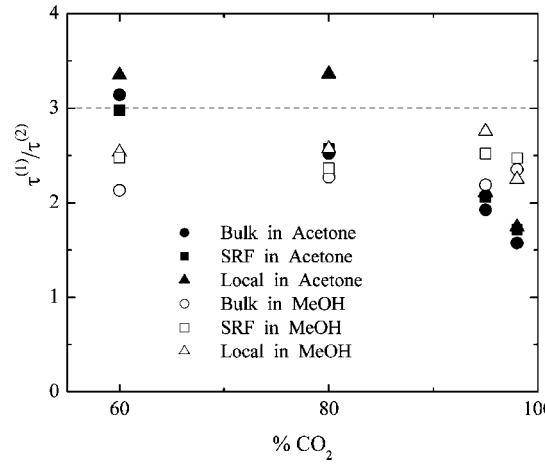

Figure 10. Ratio of the first-order and second-order total relaxation times for CO_2 molecules in acetone (filled symbols) and MeOH (open symbols) GXLs. Data are taken from Tables S1 and S2.

Most organic RCFs were fit with biexponential decay functions, although second-order MeOH RCFs were fit with triexponential decay functions, and all CO_2 RCFs were fit with single exponential decay functions. All fits had a standard error less than 2%, but most were less than 1%. RCF fitting parameters for Bulk, SRF, and Local cases for CO_2 and organic RCFs are presented in the Supporting Information. As shown in Figure 10, total decay times ($\tau^{(1)}$ in Table S1) in the first-order RCF—cf. $C^{(1)}(t)$ in eq 4—are approximately 3 times slower than the total decay times ($\tau^{(2)}$ in Table S2) in the second-order RCF—cf. $C^{(2)}(t)$ in eq 5. Solvent molecules in this system range from very fast rotors like CO_2 to relatively slow rotors like MeOH and are thereby expected to exhibit most of the range of possible responses. The ratio of 3—about which much of the data in Figure 3 lie—is typical for liquids and emerges exactly within the Debye approximation in rotational Brownian diffusion.[45] Thus the fact that the computational data yields values in agreement with this limit is an indication of the quality of the results. Moreover the total relaxation decay times are seen to lie in the range of 1 ps to 5 ps in Figure 3 that includes a significant slower component relaxation decay time. The latter is in general agreement with the total relaxation times seen in C102 in acetonitrile-water mixtures and attributed to solvent reorganization and kinetic energy transfer.[46]

The rotational relaxation is, of course, not exactly freely diffusive, and that is also indicated by the variations in the ratios of the decay times in Figure 10. The first nontrivial exponential decay time scales are similar in all three cases; however, divergence occurs at longer time scales. This indicates that a solvent molecule becomes trapped in a stable alignment with C153 and cannot freely rotate. The fast time scales are on the order of 0.1 ps as provided in Table 1 and the Supporting Information tables but do increase with increasing CO_2 composition. A similar fast decay time scale was observed by Underwood and Blank[47] for C102 in acetonitrile. They attribute this to a dipole−dipole interaction between coumarin and the solvent. That is, it is the relaxation of the direct interaction between solvent and solute for

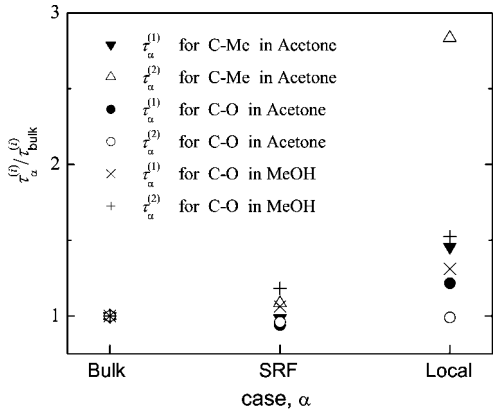

Figure 11. Normalized overall decay times calculated for every case of variable α—Bulk, SRF and Local—and averaged over solvent compositions. Values of a_i and τ_i used to determine $\tau_\alpha^{(i)}$ by eq 10 are taken from Tables S3−S6.

motions not affected by tertiary contacts. This fast relaxation mechanism is precisely the one operative in our observed simulations.

As shown in Figure 11, the general trend for the overall rotational decay times in the GXLs with the same bulk solvent composition is Bulk < SRF < Local, suggesting that C153 affects solvent rotation. These times are calculated in a manner analogous to eq 7 with $S(t)$ replaced by $C^{(i)}(t)$

$$\tau_\alpha^{(i)} = \int_0^\infty C_\alpha^{(i)}(t)\, dt = \sum_{j=1}^{k} a_{j,\alpha}^{(i)} \tau_{j,\alpha}^{(i)} \qquad (10)$$

where α denotes the corresponding solvent region—bulk, SRF or local—and is often neglected in the expressions whenever possible without loss of clarity. A possible scenario accounting for this behavior centers on the induced alignment of solvent molecules with C153 and each other self-consistently. The initial excitation traps the local solvent configuration into a local minimum energy state. The long-ranged electrostatic force induces a relaxation in the solvent structure as molecules realign with the newly formed (coarse-grained) C153 dipole moment, but molecules within the cybotactic region will "see" the charge redistribution within C153 and align accordingly. Molecules in the former will relax in an environment that is feeling a similar field that leads to an overall similar relaxation. The solvent around a molecule in the cybotactic region will be heterogeneous, relaxing at different decay rates and leading to a different self-consistent relaxation time. This argument is consistent with the presence of multiple relaxation times seen in the CRFs, and it is detailed in the fitting parameters provided in the Supporting Information. It is also consistent with the decrease in damping seen by Underwood and Blank,[47] though in their case the interaction is modulated with overall density and not relative composition.

The rotation of the C−O bond vector in acetone is initially independent of composition, although the relative contributions of each time scale (as indicated by the varying values of the pre-exponential factors in eq 6 and listed in Tables S3 and S4 of the Supporting Information) change significantly with CO_2 composition. The initial independence of composition is evident in Figure 5 where the initial rate of decay is identical in each GXL, and most variations occurred after 0.5 ps. Rotation of the C-Me vector in acetone has initial time scales that are an order-of-magnitude faster than initial rotations of the C−O vector. Longer time scales are faster than for those of the C−O vector, and the fitting parameters exhibit less variation between GXLs. This behavior shows the heterogeneous nature of acetone rotations, suggesting that the C-Me axes are the preferred axes of rotation.

First-order MeOH RCFs behave similarly to the acetone RCFs where the initial time scales vary little between GXLs and the prefactors increase with CO_2 composition. The longer time scales become significantly shorter with more CO_2 but contribute less to the overall rotation time scale. Second-order RCFs were fit with a triexponential decay function because there is a very fast initial response followed by two distinct and significant rotational times. The initial response time and contribution is very composition-dependent and most significant at higher CO_2 compositions. Long time scales decrease with increased CO_2 composition over the entire range, which indicates that MeOH-MeOH interactions do not inhibit MeOH rotation at first but become significant and hinder rotation after this brief first period. As more CO_2 is added, MeOH-MeOH hydrogen bonds are less prevalent and MeOH rotates more freely.

Solvent rotations give additional insights into the solvation behavior in GXLs and the underlying molecular interactions that affect solvation. MeOH rotations are slower than the solvation time scales in neat MeOH and 60% and 80% GXLs because of strong MeOH-MeOH hydrogen bonds. Solvation in these solvents is a function of MeOH diffusion into the cybotactic region. At very high CO_2 compositions (>95%) the rotational rates become comparable to solvation rates. In this regime the hydrogen bonding is less pronounced, and solvation is due primarily to solvent rotation and diffusion in the cybotactic region. CO_2 rotations are comparable to solvation time scales, but the nonpolar properties of CO_2 limit its contribution to solvation. Acetone rotations are less affected by composition, and rotations around both axes in neat organic and low-pressure GXLs are comparable to the solvation time scale. Rotations are much faster in high-CO_2 GXLs, so acetone diffusion into the cybotactic region determines the solvation time. The different rotational speeds about both acetone rotational axes indicate that the C-Me bond are the preferred axes rotation.

4. Conclusions

MD simulations have been used to study the solvation and rotational dynamics in two types of GXLs: CO_2-expanded acetone and MeOH. Solvation time scales are similar to those in the neat organic for compositions up to 80% CO_2 for MeOH and 60% CO_2 for acetone. Dynamics in this composition range are dominated by the organic species; a finding consistent with previous spectroscopic results where the local composition around C153 is preferentially solvated by the organic component.[21,22]

Solvation behavior is most tunable at higher CO_2 compositions, and relaxation time scales can be adjusted several ps with moderate CO_2 pressure changes.

The response of the GXL solvent to a repolarization of a solute—through, for example, electronic excitation—occurs at a range of time scales from 1 to 10 ps. The underlying motion—translational and rotational—induced by the excitation at these time scales are also comparable to the intrinsic (thermal) rotation of the solvent, and hence it is a nontrivial exercise to deconvolute their responses. Meanwhile, the collision time is just under 1 ps, and the response is certainly affected by solvent-solvent interactions in the local domain of the solute. First- and second-order rotational correlation functions have been obtained in the bulk and local solvent regimes to explore solute effects on rotation and rotational effects on solvation. Solvent rotational decay is determined by several factors: cosolvent polarity and interactions, proximity to the solute, and bulk composition. CO_2 rotations are insensitive to composition, but the two organic species depend on all factors. Acetone and MeOH rotations are faster with added CO_2 and distance from C153. MeOH rotations are hindered because of hydrogen bonds, while acetone rotations are viscosity dependent. Solvation and rotational dynamics in GXLs are relatively insensitive to composition until higher CO_2 compositions ($>80\%$). Solvation dynamics affect reaction kinetics, and the tunability of GXLs shows potential in atom transfer radical polymerizations and electron transfer through nanodevices.

Acknowledgment. This work has been supported by a Department of Energy Basic Energy Sciences grant, DE-FG02-04ER15521. C.A.E. acknowledges the support of the J. Erksine Love, Jr., Institute Chair. The computational facilities at the CCMST have been supported under NSF grant CHE 0443564.

Supporting Information Available: Detail about the computationally observed rotational correlation functions (RCF) and their associated total and partial decay times (Figures S1−S4 and Tables S1−S5). This material is available free of charge via the Internet at http://pubs.acs.org.

References

(1) Hallett, J. P.; Kitchens, C. L.; Hernandez, R.; Liotta, C. L.; Eckert, C. A. *Acc. Chem. Res.* **2006**, *39*, 531.

(2) Jessop, P. G.; Subramaniam, B. *Chem. Rev.* **2007**, *107*, 2666.

(3) Wei, M.; Musie, G. T.; Busch, D. H.; Subramaniam, B. *J. Am. Chem. Soc.* **2002**, *124*, 2513.

(4) Chamblee, T. S.; Weikel, R. R.; Nolen, S. A.; Liotta, C. L.; Eckert, C. A. *Green Chem.* **2004**, *6*, 382.

(5) Eckert, C. A.; Liotta, C. L.; Bush, D.; Brown, J. S.; Hallett, J. P. *J. Phys. Chem. B* **2004**, *108*, 18108.

(6) Xie, X. F.; Liotta, C. L.; Eckert, C. A. *Ind. Eng. Chem. Res.* **2004**, *43*, 7907.

(7) Jin, H.; Subramaniam, B.; Ghosh, A.; Tunge, J. *AIChE J.* **2006**, *52*, 2575.

(8) Fang, J.; Jin, H.; Ruddy, T.; Pennybaker, K.; Fahey, D.; Subramaniam, B. *Ind. Eng. Chem. Res.* **2007**, *46*, 8687.

(9) Nunes, R. M. D.; Arnaut, L. G.; Solntsev, K. M.; Tolbert, L. M.; Formosinho, S. J. *J. Am. Chem. Soc.* **2005**, *127*, 11890.

(10) Eckert, C.; Liotta, C.; Ragauskas, A.; Hallett, J.; Kitchens, C.; Hill, E.; Draucker, L. *Green Chem.* **2007**, *9*, 545.

(11) Myneni, S.; Hess, D. W. *J. Electrochem. Soc.* **2003**, *150*, G744.

(12) Levitin, G.; Myneni, S.; Hess, D. W. *J. Electrochem. Soc.* **2004**, *151*, G380.

(13) Anand, M.; McLeod, M. C.; Bell, P. W.; Roberts, C. B. *J. Phys. Chem. B* **2005**, *109*, 22852.

(14) McLeod, M. C.; Anand, M.; Kitchens, C. L.; Roberts, C. B. *Nano Lett.* **2005**, *5*, 461.

(15) Spuller, M. T.; Perchuk, R. S.; Hess, D. W. *J. Electrochem. Soc.* **2005**, *152*, G40.

(16) Kitchens, C. L.; Roberts, C. B. *Ind. Eng. Chem. Res.* **2006**, *45*, 1550.

(17) Song, I.; Spuller, M.; Levitin, G.; Hess, D. W. *J. Electrochem. Soc.* **2006**, *153*, G314.

(18) Anand, M.; You, S. S.; Hurst, K. M.; Saunders, S. R.; Kitchens, C. L.; Ashurst, W. R.; Roberts, C. B. *Ind. Eng. Chem. Res.* **2008**, *47*, 553.

(19) Horng, M. L.; Gardecki, J. A.; Papazyan, A.; Maroncelli, M. *J. Phys. Chem.* **1995**, *99*, 17311.

(20) Li, H. P.; Arzhantsev, S.; Maroncelli, M. *J. Phys. Chem. B* **2007**, *111*, 3208.

(21) Gohres, J.; Kitchens, C.; Hallett, J.; Popov, A.; Hernandez, R.; Liotta, C.; Eckert, C. *J. Phys. Chem. B* **2008**, *112*, 4666.

(22) Gohres, J. L.; Hernandez, R.; Liotta, C. L.; Eckert, C. A. Viewing the cybotactic structure of gas-expanded liquids. In *Green Chemistry and Engineering with Gas Expanded Liquids and Near-critical Media*; ACS Symposium Series 1006; Hutchenson, K. W., Scurto, A. M., Subramaniam, B., Eds.; American Chemical Society: Washington, DC, 2008; in press.

(23) Parsons, D. F.; Vener, M. V.; Basilevsky, M. V. *J. Phys. Chem. A* **1999**, *103*, 1171.

(24) Agmon, N. *J. Phys. Chem. A* **2002**, *106*, 7256.

(25) Egorov, S. A. *Phys. Rev. Lett.* **2004**, 93.

(26) Graf, P.; Nitzan, A. *Chem. Phys.* **1998**, *235*, 297.

(27) Egorov, S. A. *J. Chem. Phys.* **2004**, *121*, 6948.

(28) Brennecke, J. F.; Chateauneuf, J. E. *Chem. Rev.* **1999**, *99*, 433.

(29) Tsarevsky, N. V.; Pintauer, T.; Matyjaszewski, K. *Macromolecules* **2004**, *37*, 9768.

(30) Braunecker, W. A.; Matyjaszewski, K. *J. Mol. Catal., A: Chem.* **2006**, *254*, 155.

(31) Weiss, E. A.; Ahrens, M. J.; Sinks, L. E.; Ratner, M. A.; Wasielewski, M. R. *J. Am. Chem. Soc.* **2004**, *126*, 9510.

(32) Ratera, I.; Sporer, C.; Ruiz-Molina, D.; Ventosa, N.; Baggerman, J.; Brouwer, A. M.; Rovira, C.; Veciana, J. *J. Am. Chem. Soc.* **2007**, *129*, 6117.

(33) Liu, M.; Waldeck, D. H.; Oliver, A. M.; Head, N. J.; Paddon-Row, M. N. *J. Am. Chem. Soc.* **2004**, *126*, 10778.

(34) Potoff, J. J.; Siepmann, J. I. *AIChE J.* **2001**, *47*, 1676.

(35) Shukla, C. L.; Hallett, J. P.; Popov, A. V.; Hernandez, R.; Liotta, C. L.; Eckert, C. A. *J. Phys. Chem. B* **2006**, *110*, 24101.

(36) Li, H. P.; Maroncelli, M. *J. Phys. Chem. B* **2006**, *110*, 21189.

(37) Cichos, F.; Brown, R.; Bopp, P. A. *J. Chem. Phys.* **2001**, *114*, 6834.

(38) Smith, W.; Forester, T. R. *J. Mol. Graphics* **1996**, *14*, 136.

(39) Pranata, J.; Wierschke, S. G.; Jorgensen, W. L. *J. Am. Chem. Soc.* **1991**, *113*, 2810.

(40) Kumar, P. V.; Maroncelli, M. *J. Chem. Phys.* **1995**, *103*, 3038.

(41) Jorgensen, W. L. *J. Phys. Chem.* **1986**, *90*, 1276.

(42) Jorgensen, W. L.; Briggs, J. M.; Contreras, M. L. *J. Phys. Chem.* **1990**, *94*, 1683.

(43) Patel, N. C.; Teja, A. S. *Chem. Eng. Sci.* **1982**, *37*, 463.

(44) Heyes, D. M.; Powles, J. G.; Rickayzen, G. *Mol. Phys.* **2002**, *100*, 595.

(45) Hansen, J. P.; McDonald, I. R. *Theory of simple liquids*, 2nd ed.; Academic Press: London, Orlando, 1986.

(46) Wells, N. P.; McGrath, M. J.; Siepmann, J. I.; Underwood, D. F.; Blank, D. A. *J. Phys. Chem. A* **2008**, *112*, 2511.

(47) Underwood, D. F.; Blank, D. A. *J. Phys. Chem. A* **2005**, *109*, 3295.

CT800353S